ELSEVIER

Journal of Nuclear Materials 289 (2001) 167–176

journal of nuclear materials

www.elsevier.nl/locate/jnucmat

Computational study of plutonium–neodymium fluorobritholite $Ca_9Nd_{0.5}Pu_{0.5}(SiO_4)(PO_4)_5F_2$ thermodynamic properties and threshold displacement energies

C. Meis *

Commissariat à l'Energie Atomique, Centre d'Etudes de Saclay, Laboratoire d'Etudes de Physico-Chimie des Actinides, DCC/DPE/SPCP, Bât 125, 91191 Gif-sur-Yvette, France

Abstract

A force field for the modelling of neodymium fluorobritholites, having the general composition $Ca_{10-y}Nd_y(SiO_4)_y(PO_4)_{6-y}F_2$, is derived. The validity of the established analytical potentials is tested by calculating the crystallographic parameters of the compositions for $0 \leqslant y \leqslant 6$ and comparing to the experimental values. The validity is further tested by calculating the variation of the phonon spectra when transitioning from the fluoroapatite $Ca_{10}(PO_4)_6F_2$ to the full silicate neodymium fluorobritholite $Ca_4Nd_6(SiO_4)_6F_2$. Trivalent plutonium ions are introduced into the mono-silicate neodymium fluorobritholite using transferable potentials in order to obtain the composition $Ca_9Pu_{0.5}Nd_{0.5}(SiO_4)(PO_4)_5F_2$, which corresponds to a Pu concentration of about 10 wt%. The thermodynamic properties of the resulting structure are calculated, and the threshold displacement energies of various sublattices are estimated by applying the sudden approximation (SA) method. The activation energies for Frenkel defect annealing are also calculated using the rational function optimisation (RFO) procedure for the saddle point research.

PACS: 61.50.Ah; 61.80.–X; 61.80.AZ; 66.50.+m

1. Introduction

Britholites are rare-earth (RE) silicate-phosphate isomorphs of the most abundant natural apatite $Ca_{10}(PO_4)_6(F, Cl, OH)_2$ having the composition $Ca_{10-y}(RE)_y(SiO_4)_y(PO_4)_{6-y}(F, Cl, OH)_2$, where RE = Gd, Nd, La, Ce, Pm, Sm, and Eu. Previous studies on geological apatite samples [1] as well as ion beam radiation experiments [2–4] have established the inherent capacity of the fluoroapatite $Ca_{10}(PO_4)_6F_2$ to anneal radiation-induced defects at a relatively low temperature (~70°C). This property considerably decreases when increasing numbers of silicates groups $[SiO_4]^{4-}$ are substituted for phosphates $[PO_4]^{3-}$ and RE elements are substituted for calcium to charge compensate [5]. It has also been demonstrated experimentally that the temperature above which the critical amorphisation dose increases rapidly is 650 K for $Ca_2La_8(SiO_4)_6O_2$, considerably higher compared to that of the $Ca_{10}(PO_4)_6F_2$, which is 400 K [2,3]. In contrast, it is well known that silicate groups contribute to the chemical stability and durability of the apatite structure. Low silicate fluorobritholites found in the Oklo natural reactor have retained both significant quantities of ^{235}U, resulting from the α-decay of ^{239}Pu incorporated during crystallisation, and a high fission product concentration over geological time periods, conserving their crystalline state in spite of being subject to significant α-decay doses [6,7]. Actinides substitute for RE elements at calcium sites, while fission products are also readily incorporated [7,8]. Hence, low silicate fluorobritholites $Ca_{10-y}(RE)_y(SiO_4)_y(PO_4)_{6-y}F_2$ (with $y \sim 1$) have been proposed as potential host phases for Pu and HLW immobilisation [9–11].

* Tel.: +33-169 089 162; fax: +33-169 089 221.
E-mail address: cmeis@cea.fr (C. Meis).

0022-3115/01/$ - see front matter
PII: S0022-3115(00)00694-2

In this paper, we carry out a computational study, using the GULP code [12,13] and inter-atomic potential modelling, for investigating the thermodynamic properties, the threshold displacement energies and the corresponding activation energies for Frenkel defect annealing of the plutonium–neodymium mono-silicate fluorobritholite $Ca_9Pu_{0.5}Nd_{0.5}(SiO_4)(PO_4)_5F_2$. Although, for criticality reasons, gadolinium fluorobritholites $Ca_9Pu_{0.5}Nd_{0.5}(SiO_4)(PO_4)_5F_2$ could be more appropriate for Pu immobilisation, the neodymium choice in this study is simply based on the fact that the ionic radii of Nd^{3+} and Pu^{3+} are almost equal to entailing negligible lattice distortion.

2. Inter-atomic potential modelling

The fluorobritholite unit cell is hexagonal and X-rays diffraction studies [14,15] have shown the space group to be $P6_3/m$ (Fig. 1). Observations on natural samples and experimental investigations revealed the preference of neodymium ions to substitute for Ca(2), which is sevenfold co-ordinated, six oxygen ions and a fluorine, rather than for Ca(1), which is nine oxygen co-ordinated [16–20]. The Ca(2) ions are distributed in an hexagonal spiral configuration along the c axes forming tunnels of an approximate diameter of 0.4 nm whose centre is occupied by an array of fluorine ions. A recent theoretical study has shown the free energy of the system to be considerably lower when Nd ions substitute for Ca(2) [21]. A force field for the fluoroapatite $Ca_{10}(PO_4)_6F_2$ was first established, based on the experimental data of lattice parameters, ionic positions and elastic matrix elements [14,15,22,23]. Using transferable potentials, pairs of $(Nd^{3+}, [SiO_4]^{4-})$ are substituted for $(Ca^{2+}, [PO_4]^{3-})$ in the optimised fluoroapatite structure to obtain $Ca_{10-y}Nd_y(SiO_4)_y(PO_4)_{6-y}F_2$, the neodymium fluorobritholites [21]. We have used two-body ionic short-range interaction potentials of the Buckingham type supplementing the Coulomb interactions. These potentials are composed by the well-known Born–Mayer repulsive exponential term and an r^{-6} attractive one. In order to better represent the tetrahedral configuration of oxygen ions around phosphorus and silicon, two harmonic three-body short-range interaction potentials are introduced. The oxygen polarisability is taken into account by using the shell model of Dick–Overhauser [24].

The potential parameters involved in the neodymium fluorobritholite are given in Table 1. The Born–Mayer terms of the oxygen–oxygen, fluorine–fluorine, oxygen–

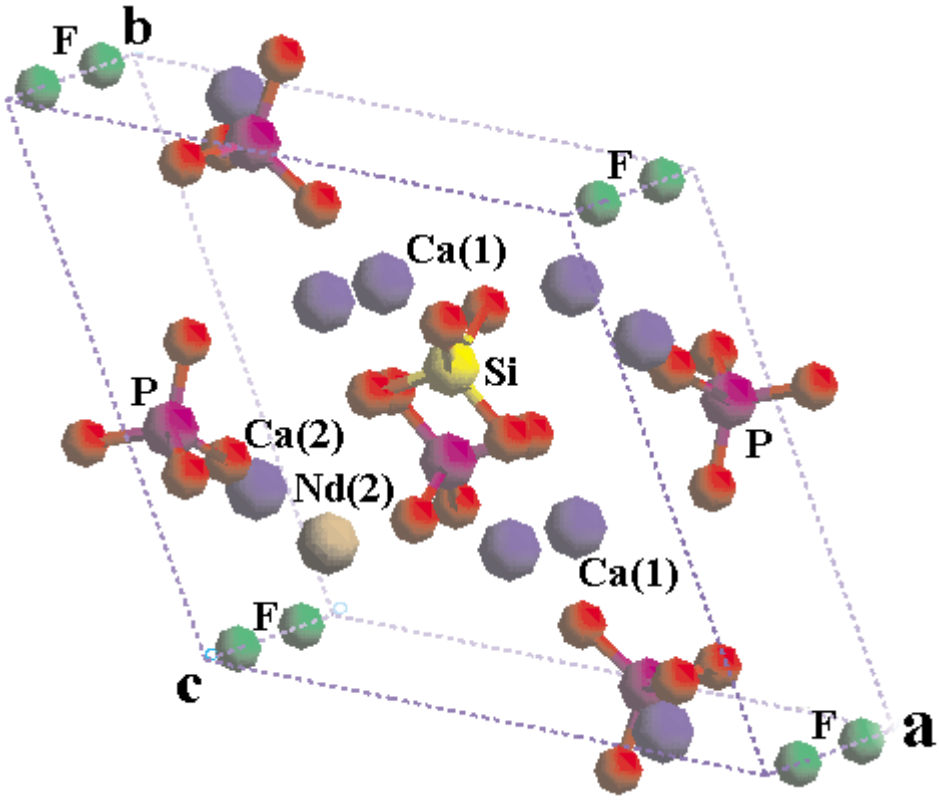

Fig. 1. Unit cell of $Ca_9Nd(SiO_4)(PO_4)_5F_2$ with the neodymium ion substituted for Ca(2).

Table 1
Potentials, parameters for plutonium–neodymium fluorobritholites

Buckingham potentials: $E = A\exp(-r/\rho) - C/r^6$ Interaction	A (eV)	ρ (nm)	C (eV nm^6)
O_{shell}–O_{shell}	22764	0.01490	32.58×10^{-6}
O_{shell}–P^{5+}_{core}	836	0.03513	
O_{shell}–Ca^{2+}_{core}	1288	0.03316	
O_{shell}–F^{-}_{core}	198	0.01110	
F^{-}_{core}–P^{5+}_{core}	697	0.02389	
F^{-}_{core}–Ca^{2+}_{core}	2031	0.02711	
F^{-}_{core}–F^{-}_{core}	1128	0.02753	
O_{shell}–Si^{4+}_{core}	1078	0.03237	
O_{shell}–Nd^{3+}_{core}	1380	0.03604	
F^{-}_{core}–Si^{4+}_{core}	3506	0.02251	
F^{-}_{core}–Nd^{3+}_{core}	89596	0.01983	
O_{shell}–Pu^{3+}_{core}	3250	0.03136	
F^{-}_{core}–Pu^{3+}_{core}	3058	0.02865	

Three-body harmonic: $E_{ijk} = \frac{1}{2}k_{ijk}(\theta - \theta_0)^2$
$k_{O_{shell}-P-O_{shell}} = 2.840$ eV rad^{-2}; $\theta_0 = 109.5°$
$k_{O_{shell}-Si-O_{shell}} = 16.67$ eV rad^{-2}; $\theta_0 = 110.4°$
Oxygen charges: O_{core}: +0.860; O_{shell}: −2.860
Polarisability: $E_P = \frac{1}{2}K_P r^2_{core-shell}$
$K_P(O_{core}–O_{shell}) = 9867$ eV nm^{-2}

fluorine and oxygen–neodymium two-body interactions were fixed at the values published previously [25–28]. The calculated lattice parameters of the neodymium fluorobritholites are represented in Table 2 and show good agreement with the experimental values. The calcium–oxygen distances, as well as the phosphate groups bond angles of the relaxed structures, are also in satisfactory agreement with the experimental values [21]. To check further the quality of the force field, we have calculated the phonon frequencies ν_i from the eigenvalues of the dynamic matrix of the system, corresponding to the Cartesian second derivatives of the energy weighted by the inverse square root of the ion masses. The frequencies attributed to the phosphate groups of $Ca_{10}(PO_4)_6F_2$ and to the silicate groups of $Ca_4Nd_6(SiO_4)_6F_2$ are given in Table 3 and compared to the experimental values, also showing a reasonable agreement on the whole.

Plutonium ions are introduced in the mono-silicate ($y = 1$) neodymium fluorobritholite using again transferable potentials (Table 1) but respecting the transferability constraints [21]. A Pu^{3+} ion is substituted for Nd^{3+} every two unit cells of $Ca_9Nd(SiO_4)(PO_4)_5F_2$ {a,b,2c} to get $Ca_9Nd_{0.5}Pu_{0.5}(SiO_4)(PO_4)_5F_2$ corresponding to a plutonium concentration of about 10 wt%. Free energy calculations with Pu^{3+} substituted for Nd^{3+} at Ca(2) and Ca(1) sites, respectively, revealed the tendency of the plutonium ions to occupy preferentially Ca(2) sites [21]. In order to avoid the unphysical symmetric configuration, resulting when Pu^{3+}, Nd^{3+} and $[SiO_4]^{4-}$ are located periodically at the same co-ordinates in each lattice along the a and b axes, as we use periodic boundary conditions, we have considered the unit cell of the composition $Ca_9Pu_{0.5}Nd_{0.5}(SiO_4)$ $(PO_4)_5F_2$ to be composed of eight unit cells {2a,2b,2c} of $Ca_9Pu_{0.5}Nd_{0.5}(SiO_4)(PO_4)_5F_2$, that is $Ca_{72}Pu_4Nd_4$ $(SiO_4)_8(PO_4)_{40}F_{16}$. In this supercell,

Table 2
Calculated and experimental (in parentheses [15]) lattice parameters for the neodymium fluorobritholites $Ca_{10-y}Nd_y(SiO_4)_y(PO_4)_{6-y}F_2 (0 \leqslant y \leqslant 6)$

$Ca_{10-y}Nd_y(SiO_4)_y(PO_4)_{6-y}F_2$	a (nm)	%	c (nm)	%	V (nm^3)	%
$Ca_{10}(PO_4)_6F_2$	0.9368(0.9374)	−0.05	0.6886(0.6869)	−0.27	0.522(0.524)	−0.38
$Ca_9Nd(SiO_4)(PO_4)_5F_2$	0.9438(0.9405)	+0.26	0.6851(0.6906)	−0.79	0.526(0.529)	−0.41
$Ca_8Nd_2(SiO_4)_2(PO_4)_4F_2$	0.9480(0.9438)	+0.44	0.6888(0.6938)	−0.72	0.533(0.535)	−0.35
$Ca_7Nd_3(SiO_4)_3(PO_4)_3F_2$	0.9502(0.9476)	+0.27	0.6926(0.6964)	−0.56	0.538(0.540)	−0.22
$Ca_6Nd_4(SiO_4)_4(PO_4)_2F_2$	0.9573(0.9494)	+0.83	0.6901(0.6981)	−1.14	0.542(0.545)	−0.49
$Ca_5Nd_5(SiO_4)_5(PO_4)F_2$	0.9592(0.9508)	+0.88	0.6913(0.6996)	−1.18	0.545(0.548)	−0.44
$Ca_4Nd_6(SiO_4)_6F_2$	0.9591(0.9527)	+0.68	0.6939(0.7013)	−1.06	0.549(0.551)	−0.42

Table 3
Phonon frequencies (experimental in parentheses [15]) for the phosphate groups in $Ca_{10}(PO_4)_6F_2$ and the silicate groups in $Ca_4Nd_6(SiO_4)_6F_2$

ν (cm^{-1})	$Ca_{10}(PO_4)_6F_2$	$Ca_4Nd_6(SiO_4)_6F_2$
ν_1	968 (964)	902 (884)
ν_2	471 (469)	418–476 (406–459)
ν_3	1045–1094 (1032–1088)	931–981 (924–962)
ν_4	565–603 (512–593)	511–554 (500–542)

adopting the P1 translation symmetry group with the Cartesian y and z axes along the b and c, respectively (Fig. 2), silicates are substituted for phosphates at random positions, while 75% of Pu and Nd ions are substituted for Ca(2) and 25% for Ca(1), in conformity with the previous theoretical and experimental studies [16–21].

3. Thermodynamic properties

After relaxing the system at constant pressure, applying the Newton-Raphson optimisation method with BFGS Hessian update, we have calculated the phonon frequencies ν_i to obtain the partition function:

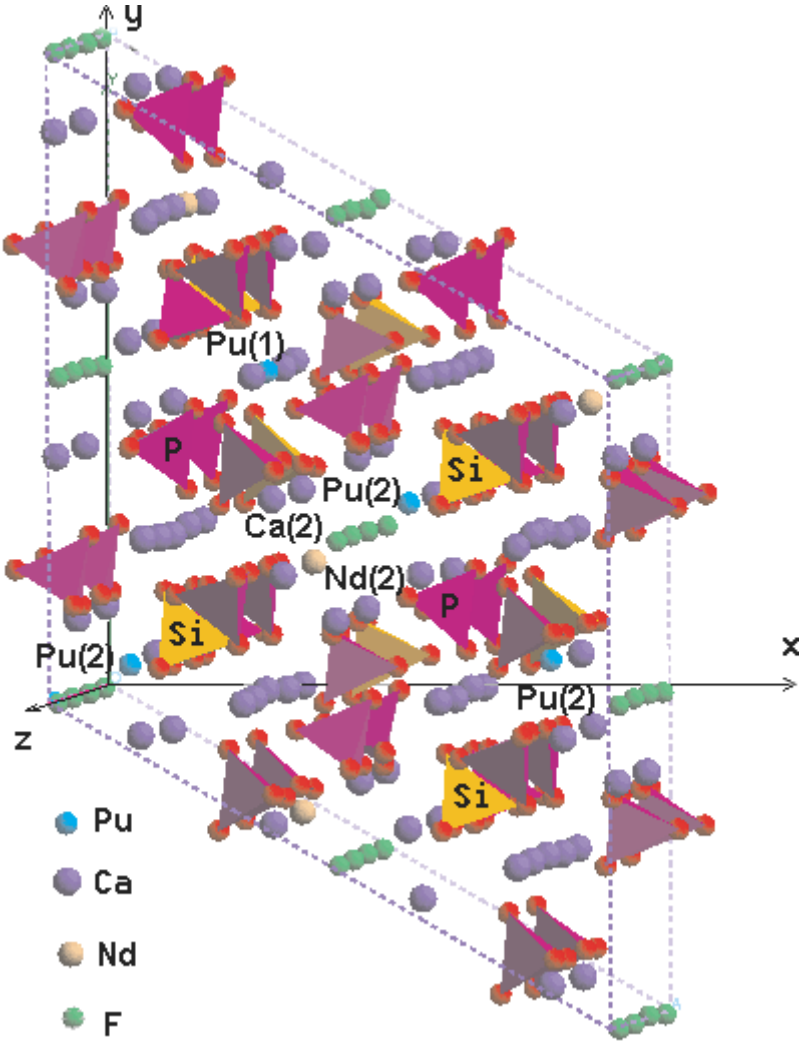

Fig. 2. Plutonium distribution in the fluorobritholite $Ca_{72}Pu_4Nd_4(SiO_4)_8(PO_4)_{40}F_{16}$. Pu(1) is plutonium at site 1 and Pu(2) at site 2.

$$Z_{\text{vib}} = \sum_{k\,\text{points}=6} g_k \sum_{i=1}^{3N} \exp(-hv_i/k_B T), \tag{1}$$

where the summation runs over a grid covering 6 k symmetry-unique points across the Brillouin zone, excluding the three translational degrees of freedom at the gamma point. The parameter g_k is the weight of each grid point and N is the total number of ions in the simulation volume, which is a single unit cell of $Ca_{72}Pu_4Nd_4(SiO_4)_8(PO_4)_{40}F_{16}$ with periodic boundary conditions. Also, k_B and h are the Boltzmann's and Planck's constants, respectively. The vibration entropy is immediately obtained by the well-known relation:

$$S_{\text{vib}} = k_B \ln Z_{\text{vib}} + k_B T \frac{\partial}{\partial T}(\ln Z_{\text{vib}}) \tag{2}$$

and the specific heat at constant pressure:

$$C_P = T \left.\frac{\partial S_{\text{vib}}}{\partial T}\right|_P. \tag{3}$$

The polynomial fittings of the calculated C_P in the temperature range 20–800°C for $Ca_9Nd_{0.5}Pu_{0.5}(SiO_4)(PO_4)_5F_2$ and $Ca_{10}(PO_4)_6F_2$ are plotted in Fig. 3, together with the experimental values for the fluoroapatite [21]. The calculated C_P, S_{vib} and the bulk modulus, B, at 300 K are given in Table 4, as well as the fusion temperatures T_f, calculated by molecular dynamics (MD). It is worth noting that the thermodynamic properties of $Ca_9Nd_{0.5}Pu_{0.5}(SiO_4)(PO_4)_5F_2$ are very close to those of the fluoroapatite $Ca_{10}(PO_4)_6F_2$, though the bulk modulus is larger by roughly 10%. In general, MD simulations overestimate the fusion temperature since surface effects are neglected. Also, the error due to the type of the force field used and due to the simulation noise may be important. Despite this, the calculated T_f for $Ca_{10}(PO_4)_6F_2$ is about 7% higher than the real value demonstrating further the efficiency of the established shell-model potentials. However, the fusion temperature obtained for $Ca_9Nd_{0.5}Pu_{0.5}(SiO_4)(PO_4)_5F_2$ only shows the tendency to be higher than that of the fluoroapatite by 100–200° (roughly 10%). In fact, the numerical difference between the calculated fusion temperatures of these two structures is relatively small to be considered as an absolute value, and can be easily absorbed in the simulation noise.

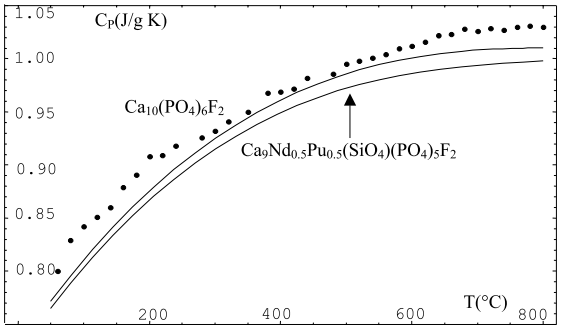

Fig. 3. Calculated specific heat at constant pressure, C_P, for the fluoroapatite and for the neodymium–plutonium mono-silicate fluorobritholite. Dots are the experimental measures for the fluoroapatite [21].

4. Threshold displacement energies and defect migration

The α-particle and principally the recoil nucleus produced during the α-decay process are the primary sources of atomic displacements in ceramics proposed for HLW immobilisation. In the case of Pu-doped materials, the decay of ^{239}Pu releases a 5.2 MeV α-particle and an 86 keV ^{235}U recoil nucleus. Most of the α-particle energy is dissipated by electronic excitation and ionisation over long distances, of about 20 μm, producing roughly 100–200 atomic displacements at the end of the path [6]. Conversely, for the massive ^{235}U, the nuclear stopping power is much more significant than the electronic one. Consequently, the elastic collisions of the α-decay recoiling atom with the ions of the lattice are mainly responsible for a high degree of damage in the material [30–34].

As it is well known, the threshold displacement energy is defined as the minimum kinetic energy transferred to a lattice atom, the so-called primary knock-on atom (PKA), yielding the creation of a stable Frenkel defect. Hence, this parameter is of crucial importance for quantifying the number of displaced atoms produced in radiation cascades and provides basic information for modelling radiation effects in materials.

A large number of experimental and theoretical studies have permitted establishing reliable E_d values in various metallic compounds [35–38]. It is generally accepted that the number of Frenkel defects created in a metal due to a particle with available kinetic damage

Table 4
Calculated (rounded to the nearest integer) properties for fluoroapatite and neodymium–plutonium mono-silicate fluorobritholite[a]

Apatite	T_f (°C)	B (GPa)	C_P (J/mol K)	S_{vib} (J/mol K)
$Ca_{10}(PO_4)_6F_2$	(1640) 1750	92 (98)	742 (765 ± 12)	808 (775)
$Ca_9Pu_{0.5}Nd_{0.5}(SiO_4)(PO_4)_5F_2$	~1850	103	725	791

[a] The values for the C_P, B and S_{vib} are given at 300 K. In parentheses the experimental values [15,21,22,29].

energy $E_{\mathrm{kin}}^{\mathrm{dam}}$ (inelastic losses subtracted) is obtained by the NRT expression [39]:

$$N_{\mathrm{Frenkeldef}} = \frac{0.8E_{\mathrm{kin}}^{\mathrm{dam}}}{2E_{\mathrm{d}}}, \tag{4}$$

where the empirical factor 0.8 accounts for the fact that ions do not behave as perfect hard spheres during collisions. Conversely, quite a few E_{d} values are available for ceramic materials under consideration as matrices for radionuclides immobilisation. None of these quantities are known for apatites, hence, the purpose of this computational study is to obtain a general picture for the composition that we are interested in, $Ca_9Nd_{0.5}Pu_{0.5}(SiO_4)(PO_4)_5F_2$. The major complication arises from the fact that ceramics generally consist of multiple sublattices and consequently the threshold displacement energies should be determined for each one in various crystallographic directions. In our case, the plutonium–neodymium mono-silicate fluorobritholite is almost composed by as many sublattices as the total number of atoms in the unit cell $Ca_{72}Pu_4Nd_4(SiO_4)_8(PO_4)_{40}F_{16}$. This is mainly due to the high complexity of the apatite structure and also due to the random distribution of silicates, neodymium and plutonium. This is illustrated in Fig. 2 where, for instance, each Ca(2) ion located around the fluorine arrays in the tunnel meets a quite different environment when displaced along the main crystallographic directions. Nevertheless, we will assume here that an effective displacement energy can be defined by the relation [40]:

$$E_{\mathrm{d}}^{\mathrm{eff}} = \left[\sum_i \frac{s_i}{\langle E_{\mathrm{d}}^i\rangle_{[uvw]}}\right]^{-1}, \tag{5}$$

where s_i is the stoichiometric fraction and $\langle E_{\mathrm{d}}^i\rangle_{[uvw]}$ is the mean value of the E_{d} over different crystallographic directions and for different initial positions of the i sublattice. In reality, the parameter s_i cannot take into account the different environments of the same sublattices, however, the last expression has been derived empirically [41] for the multi-component ceramic $MgAl_2O_4$ and provides a quite satisfactory estimate of the total number of displacements when it is used with the NRT model (Eq. (4)).

The $E_{\mathrm{d}_{[uvw]}}^i$ can be calculated either by MD or by the sudden approximation (SA) within the Mott–Littleton model. In the MD method [38], the system is kept at constant temperature and volume while a definite momentum is conferred to the PKA in a given [uvw] direction. After an evolution of a few picoseconds, generally 10–100 ps, depending on the problem at hand, the system is examined to determine whether the PKA is permanently displaced or not. However, applying shell-model MD is extremely expensive as the time-step for the integration of Newton's equations of motion should be very short, of the order of 0.1 fs, in order to ensure that there is no energy transfer between shell vibrations and real modes according to the finite mass algorithm based on the Carr–Parrinello method [42,43]. Now, the PKA displacement process occurs in a time interval much shorter than that needed for phonons to relax the lattice. In fact, in the non-relativistic limit, the velocity of the α- recoil ^{235}U nucleus is $[172\ \mathrm{keV/m}(^{235}U)]^{1/2} \sim 0.3\ \mathrm{nm\ fs^{-1}}$, considerably higher than that of the ionic oscillation displacement due to the phonon vibrations in the lattice. Consequently, during the collision of the recoiling atom with the PKA it can be assumed, as a first approximation, that the vibration motion is frozen. This is the basis of the SA method [44] which does not take into account neither the dynamic effect of the PKA displacement nor the mass ratio effects (heavier/lighter ions) during collisions. However, previous studies on Si and SiC [45], as well as on zircon [46,47], revealed the E_{d} values calculated with the SA method to be comparable to those calculated with the MD simulations within about 15–20%. Thus, the application of the SA method, which is considerably less expensive than the shell-model MD, will permit obtaining a first idea of the threshold displacement energies in $Ca_9Nd_{0.5}Pu_{0.5}(SiO_4)(PO_4)_5F_2$. In the SA method, only static total energy calculations are considered. The PKA is displaced in a given crystallographic direction calculating at each position the total energy of the unrelaxed system. The E_{d} is obtained by the difference between the highest energy maximum, beyond which the ion will occupy a stable interstitial position after relaxation, and the energy of the undisturbed crystal:

$$E_{\mathrm{d}_{[uvw]}}^i = E_{\mathrm{unrelaxed}}^{\max}(\text{bulk with the } i \text{ sublattice displaced in } [uvw]) - E_{\mathrm{relaxed}}(\text{perfect bulk}). \tag{6}$$

To verify the stability of the created Frenkel defect, the system is relaxed checking whether the displaced atom moves back to its initial position. Therein, caution has to be taken when relaxing the system to avoid falling on metastable states. For avoiding such a situation, we have used the rational function optimisation (RFO) or eigenvector following, since it is considered as the most reliable method to determine real energy minima as well as n-order transition states [48]. In the RFO minimisation procedure, the investigation of the energy minima or of the saddle points is carried out by checking systematically the nature and the number of the eigenvalues of the Hessian, the energy second derivatives matrix.

The calculation is carried out here within the Mott-Littleton approximation [49]. According to this method, the region surrounding the defect centre is separated into three successive areas. The inner one is a sphere of radius r_1 in which all inter-ionic interactions are treated

rigorously and the species are allowed to relax fully. In the middle one, represented by the space between the first sphere and a second one of radius $r_2 > r_1$, species are supposed to be slightly affected by the presence of the defect located in the centre of the inner sphere and by this way only harmonic relaxations are considered. In the area outside the second sphere, ions interact with the defect as in a perfect dielectric medium.

Shown in Fig. 4(a) is a typical illustration of the translation of a Ca(1) ion along the [0 1 0] direction,

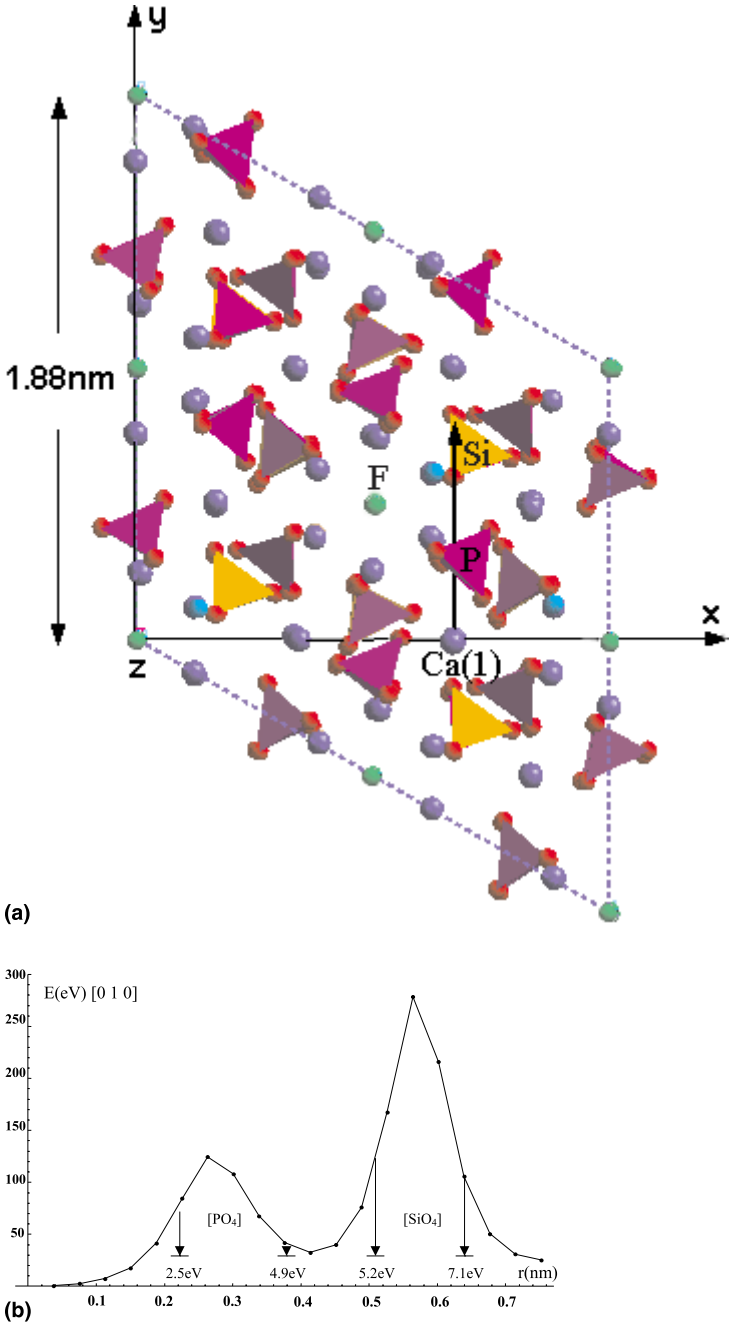

Fig. 4. (a) Displacement of a Ca(1) along the [0 1 0] direction over a distance of 0.8 nm. (b) Unrelaxed defect energy, Ca vacancy + self-interstitial. The maxima correspond to the configurations with the displaced calcium ion brushing, respectively, the phosphate and silicate tetrahedra. Arrows indicate close and extended Frenkel pair formation, after RFO relaxation, and the corresponding defect energies.

defined as in Fig. 2, over a distance of 0.8 nm while in Fig. 4(b) the corresponding calculated energy values of the unrelaxed defect are presented. The maxima correspond to the positions where the calcium ions pass successively a phosphate and a silicate tetrahedron, the last one presenting greater rigidity. The RFO relaxation at each point determines the stable interstitial positions, corresponding to the formation of close and extended Frenkel pairs, the last ones being possible only if the PKA has sufficient kinetic energy. Notice that the stable positions, depending strictly on the local energy gradients, are not necessarily located exactly on the [0 1 0] direction. The corresponding Frenkel pair E_F^i energies are calculated by:

$$E_F^i = E_{\text{relaxed}}(\text{bulk with } i \text{ vacancy and self-interstitial}) - E_{\text{relaxed}}(\text{perfect bulk}). \quad (7)$$

The threshold displacement energy for this specific Ca(1) is $E_d^{Ca(1)}[0\,1\,0] = 36$ eV, since this is the minimum energy for the formation of the close Frenkel pair. The defect surviving can be characterised by calculating the activation energy ε_{th}^i for the displaced sublattice i to an interstitial position to migrate towards the self-vacancy [50–53]. In fact, the relaxed system with the Frenkel pair constitutes the starting file for an RFO saddle point research. This situation is illustrated in Fig. 5 for the above displaced Ca(1). The close Frenkel pair formation energy is $E_F^{Ca(1)} = 2.5$ eV, while the annealing activation energy is $\varepsilon_{th}^{Ca(1)} = 0.6$ eV.

We have applied the SA within the Mott–Littleton method for calculating the $E_{d_{[uvw]}}^i$ in a few representative directions for the different sublattices of $Ca_{72}Pu_4Nd_4(SiO_4)_8(PO_4)_{40}F_{16}$, as well as the corresponding E_F^i and ε_{th}^i. The results obtained, with $r_1 = 0.9$ nm and $r_2 = 2.2$ nm, are given in Table 5, in which the different values for the same ion in a given direction correspond to different initial co-ordinates.

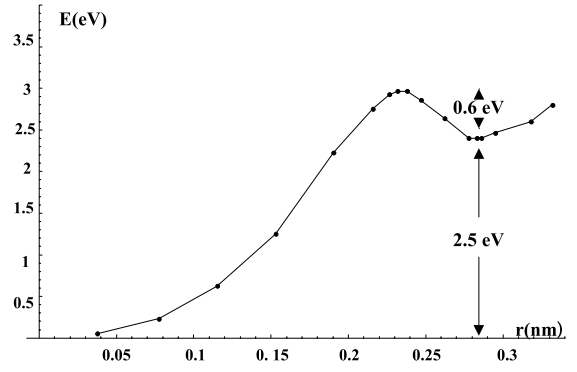

Fig. 5. Close Frenkel defect $E_F = 2.5$ eV for the Ca(1) displaced along the [0 1 0] direction. The calculated activation energy for annealing is $\varepsilon_m = 0.6$ eV.

Though we have not carried out an exhaustive study based on the values obtained and applying Eq. (5) we can get an effective displacement energy $E_d^{eff} = 32$ eV and a mean activation energy for thermal annealing $\langle \varepsilon_{th} \rangle = 0.9$ eV. Using Eq. (4), the number of displaced atoms during the release of a 86 keV ^{235}U atom in $Ca_9Nd_{0.5}Pu_{0.5}(SiO_4)(PO_4)_5F_2$ should be roughly 1100. By virtue of comparison, the effective displacement energy calculated for zircon ($ZrSiO_4$) is $E_d^{eff} = 48$ eV. This value is obtained by applying the SA method as described above, using the already published potentials [54], and by considering the displacements for Zr along [0 1 0] and [1 2 0] directions, for O along [2 5 2] and $[0\,2\,\bar{1}]$, and for Si along [1 0 0], as in [46]. In zircon, Eq. (4) yields about 720 atomic displacements during the ^{235}U release. However, the corresponding Frenkel annealing activation energies seem to be considerably higher, of the order of 2.5 eV.

5. Conclusion and discussion

The plutonium–neodymium mono-silicate fluorobritholite $Ca_9Nd_{0.5}Pu_{0.5}(SiO_4)(PO_4)_5F_2$ with 10 wt% of Pu is modelled using inter-atomic potentials. The fusion temperature and the bulk modulus are estimated to be about 10% higher than those of the fluoroapatite and the constant pressure specific heat to be 2–4% lower, depending on the temperature interval.

The calculation of the threshold displacement energies gives the general picture that amorphisation in $Ca_9Nd_{0.5}Pu_{0.5}(SiO_4)(PO_4)_5F_2$ should mainly occur by the high number of displacements of the F, and Ca, sublattices and in a second degree by those of Nd and Pu around the silicate and phosphate groups, the latter presenting a high resistance to displacement. In fact, considerable energy is needed for the displacement of phosphorus, and particularly silicon. This is explained by the rigidity of the corresponding tetrahedra essentially due to the two-body P–O and Si–O interactions rather than due to the three-body potentials O–P–O and O–Si–O used, respectively, in $[PO_4]^{3-}$ and $[SiO_4]^{4-}$. In fact, it is well known that the energy between N ions in a solid can be developed in terms of n-body interactions:

$$E(1 \ldots N) = \sum_i E_i + \sum_{i,j} E_{ij} + \sum_{i,j,k} E_{ijk} + \sum_{i,j,k,l} E_{ijkl} + \cdots$$

Hence, the three-body term is a small correction to the local energy permitting to better describe the angular distribution of oxygen ions around phosphorus and silicon in the corresponding tetrahedra. It is also worth noting that the activation energies for phosphorus and silicon Frenkel defects annealing are extremely difficult

Table 5
Threshold displacement energies E_d calculated over various crystallographic directions for the composition $Ca_9Nd_{0.5}Pu_{0.5}(SiO_4)(PO_4)_5F_2$[a]

[*uvw*]	E (eV)	Ca(1)			Ca(2)		P	Nd(2)	Si		O		F	Pu(2)
[0 1 0]	E_d	36	25	37	23	44	91	37	109	32	38	43	12	41
	E_F	2.5	2.2	2.6	2.2	2.0	12.4	9.5	11.8	2.9	1.8	3.6	2.0	12.8
	ϵ_{th}	0.6	0.7	0.5	–	1.0	2.8[b]	1.1	–	1.1	0.9	0.8	0.3	1.2
[4 $\bar{2}$ 0]	E_d	23			24		73	35	81	24		47	8	38
	E_F	3.8			7.8		13.2	8.7	12.3	4.1		3.7	1.5	11.3
	ϵ_{th}	0.8			1.2		–	1.2	–	1.0		–	0.3	1.4
[1 1 1]	E_d	19		23		30	84	32		42		53	14	36
	E_F	6.4		7.3		3.8	12.9	9.1		2.8		4.5	1.9	12.8
	ϵ_{th}	0.9		1.1		0.6	2.6	–		1.0		1.6	0.4	–
[2 5 1]	E_d	34	28	26		30	65	43	78	24	32	41	10	47
	E_F	4.8	4.6	3.7		7.2	12.1	8.2	12.1	3.1	4.6	2.7	1.7	11.0
	ϵ_{th}	0.8	0.6	0.7		1.2	–	1.1	3.7[b]	0.6	1.2	–	0.5	1.2
[1 1 0]	E_d	33			41			47		34		39		52
	E_F	5.1			2.2			9.6		3.5		3.2		12.7
	ϵ_{th}	0.7			0.6			1.0		1.1		0.7		0.9
[3 1 0]	E_d	25			28		81		98	28	36	39	9	
	E_F	4.0			3.9		13.0		8.9	2.7	3.2	2.1	2.1	
	ϵ_{th}	0.7			1.0		2.4[b]		–	0.8	1.1	0.4	–	
[$\bar{1}$ $\bar{1}$ 0]	E_d	26			32			33	86	22		35	6	40
	E_F	3.7			7.8			10.2	9.1	2.5		2.9	1.1	11.9
	ϵ_{th}	1.0			0.9			1.4	–	1.0		0.7	0.2	1.3
Average	$\langle E_d \rangle$	29					78	37	91	36			10	42
	$\langle \epsilon_h \rangle$	0.7					2.6[b]	1.1	3.7[b]	0.9			0.3	1.2

[a] The different values for the same ion in a given direction correspond to different initial co-ordinates. The $\langle E_d \rangle$ are rounded to the nearest integer. E_F and ϵ_{th} are the corresponding Frenkel defect formation energies and activation energies for annealing, respectively.
[b] Convergence not well defined.

to be determined by RFO. This is mainly due to the complex lattice rearrangement after relaxation, preventing the P or Si Frenkel pairs from annealing in one step.

The relatively low activation energies for thermal annealing mean that significant number of F and Ca close Frenkel pairs, created in the primary ballistic process, should rearrange after the end of the local thermal spike induced by the PKA displacement [55].

The radiation-induced annealing [56–58] has not been considered here. In the latest process, perturbations by charged particles (α, electrons, ...) could supply the necessary activation energy to the interstitial atom to overcome the migration potential barrier towards its initial lattice position. This could happen either by a direct interaction between the charged particle and the displaced ion, or by the intermediate of the phosphate groups. In fact, most of the interstitial positions are inevitably situated near phosphate tetrahedra whose vibration frequencies are considerably high ($\nu_1 = 968$ $cm^{-1} = 0.12$ eV). The energy of the phosphate groups, electronic excitation, when crossed by charged particles, might be transferred to higher vibration modes and, by collisions, to the displaced ion nearby acquiring the necessary energy for returning to its initial position. Therein, the coupling between the excited electronic states of phosphates and silicates to the vibration modes is worth investigating by first principles calculations, since this process may contribute to the defect annealing at low temperatures, entailing probably a local thermalisation.

The consideration of the radiation-induced annealing and a more detailed study of the extended Frenkel defect thermal recovery are necessary to complete the present study before establishing an α-decay kinetics model describing the evolution of the $Ca_9Nd_{0.5}Pu_{0.5}(SiO_4)(PO_4)_5F_2$ crystal state over storage time periods.

References

[1] G.A. Wagner, G.M. Reimer, Earth. Planet. Sci. Lett. 14 (1972) 263.
[2] R.C. Ewing, W.J. Weber, L.M. Wang, J. Mater. Res. 9 (1994) 688.

[3] W.J. Weber, L.M. Wang, Nucl. Instrum. and Meth. B 91 (1994) 63.
[4] A. Meldrum, L.M. Wang, R.C. Ewing, Nucl. Instrum. and Meth. B 116 (1996) 220.
[5] J. Carpena, in: P. Van den Haute, de Corte (Eds.), Advances in Fission Track Geochronology, Kluwer Academic Publishers, Dordrecht, 1998, 91–92.
[6] W.J. Weber, R.C. Ewing, C.R.A. Catlow, T. Diaz de la Rubia, L.W. Hobbs, C. Kinoshita, Hj. Matzle, A.T. Motta, M. Nastasi, E.K.H. Salje, E.R. Vance, S.J. Zinkle, J. Mater. Res. 13 (6) (1998).
[7] R. Bros, J. Carpena, V. Sere, A. Beltritti, Radiochim. Acta 74 (1996) 277.
[8] J. Carpena, V. Sère, in: Proceedings Fourth Joint EC-CEA Final Meeting, Saclay, 1995, pp. 225–238.
[9] J. Carpena, J.L. Lacout, Licence (1993).
[10] R.C. Ewing, W.J. Weber, W. Lutze, in: E.R. Merz, C.E. Walter (Eds.), Disposal of Weapons Plutonium, Kluwer Academic Publishers, The Netherlands, 1996, p. 65.
[11] L. Boyer, J. Carpena, J.L. Lacout, Licence (1998).
[12] J.D. Gale, J. Chem. Soc. Faraday Trans. 93 (1997) 629.
[13] J.D. Gale, Philos. Mag. B 73 (1996) 3.
[14] L. Boyer, J. Carpena, J.L. Lacout, Solid State Ionics 95 (1996) 121.
[15] L. Boyer, Thesis, Institut National Polytechnique de Toulouse, France, 7 July 1998.
[16] M.E. Fleet, Y. Pan, J. Solid State Chem. 112 (1994) 78–81.
[17] G.J. Blasse, J. Solid State Chem. 14 (1975) 181.
[18] J. Lin, Q. Su, J. Alloys and Compounds 210 (1994) 159.
[19] J. Lin, Q. Su, Mater. Chem. Phys. 38 (1994) 98.
[20] L. Boyer, J.M. Savariault, J. Carpena, L.L. Lacout, Acta Cryst. C 54 (1998) 1057.
[21] C. Meis, J.D. Gale, L. Boyer, J. Carpena, D. Gosset, J. Phys. Chem. A 104 (2000) 22.
[22] R.F.S. Hearnon, Adv. Phys. 5 (1956) 323.
[23] K. Sudarsanan, P.E. Mackie, R.A. Young, Mater. Res. Bull. 7 (1972) 1331.
[24] B.G. Dick, A.W. Overhauser, Phys. Rev. 112 (1958) 90.
[25] C.R.A. Catlow, Proc. R. Soc. Lond. A 353 (1997) 533.
[26] C.R.A. Catlow, K.M. Diller, M.J. Norgett, J. Phys. C 10 (1979) 1395.
[27] S. D'Arco, M.S. Islam, Phys. Rev. B 55 (1997) 3141.
[28] G.V. Lewis, C.R.A. Catlow, J. Phys. C 18 (1985) 1149–1161.
[29] Mazelsky et al., J. Cryst. Growth 3 (4) (1968) 360.
[30] W.J. Weber, F.P. Roberts, Nucl. Technol. 60 (1983) 178.
[31] Hj. Matzke, Nucl. Instrum. and Meth. B 32 (1988) 453.
[32] W.J. Weber, J. Minerals, Met. Mater. Soc. 43 (7) (1991) 35.
[33] W.J. Weber, L.K. Mansur, F.W. Clinard, D.M. Parkin Jr., J. Nucl. Mater. 184 (1991) 1.
[34] R.C. Ewing, W.J. Weber, F.W. Clinard, J. Prog. Nucl. Energy 29 (2) (1995) 63.
[35] T. Diaz de la Rubia, N. Soneda, M.J. Caturla, E.A. Alonso, J. Nucl. Mater. 251 (1997) 13.
[36] R.E. Stoller, G.R. Odette, B.D. Wirth, J. Nucl. Mater. 251 (1997) 49.
[37] D.J. Bacon, A.F. Calder, F. Gao, J. Nucl. Mater. 251 (1997) 1.
[38] H.O. Kitchner, L.P.Kubin, V. Pontikis (Eds.), Computer Simulation in Materials Science, NATO ASI Series, vol. 308, 1995.
[39] M.J. Norgett, M.T. Robinson, I.M. Thorrens, Nucl. Eng. Des. 33 (1975) 50.
[40] S.J. Zinkle, C. Kinoshita, J. Nucl. Mater. 251 (1997) 200.
[41] N.M. Ghoniem, S.P. Chou, J. Nucl. Mater. 155-157 (1988) 1263.
[42] R. Car, M. Paririnello, Phys. Rev. Lett. 55 (1985) 2471.
[43] P.J. Lindan, Mole. Simulation 14 (1995) 303.
[44] R.D. Levine, R.B. Bernstein, Mole. React. Dyn., Oxford University, New York, 1974.
[45] W. Windl, T.J. Lenosky, J.D. Kress, A.F. Voter, Nucl. Instrum. and Meth. B 141 (1996) 61.
[46] R.E. Williford, R. Devanathan, W.J. Weber, Nucl. Instrum. and Meth. B 141 (1998) 94.
[47] J.P. Crocombette, D. Ghaleb, J. Nucl. Mater., submitted.
[48] A. Banarjee, N. Adams, J. Simons, R. Shepard, J. Phys. Chem. 89 (1985) 52.
[49] N.F. Mott, M.J. Littleton, Trans. Faraday Soc. 34 (1938) 485.
[50] W. Jost, Diffusion, Academic, New York, 1960.
[51] T. Sonoda, C. Kinoshita, Y. Isobe, Ann. Phys. C 20 (3) (1995) 33.
[52] C. Kinoshita, K. Hiyashi, T.E. Mitchell, in: W.D. Kingery (Ed.), Structure and Properties of MgO and Al_2O_3 Ceramics, Advances in Ceramics, vol. 10, American Ceramic Society, Columbus, OH, 1984, p. 490.
[53] S.J. Zinkle, in: I.M. Robertson et al. (Eds.), Microstructure Evolution During Irradiation, Mater. Res. Soc. Symp. Proc., vol. 439, MRS, Pittsburgh, PA, 1997, p. 667.
[54] C. Meis, J.D. Gale, Mater. Sci. Eng. B 57 (1998) 52.
[55] L.A. Miller, D.K. Brice, A.K. Prinja, S.T. Picraux, Phys. Rev. B 49 (1994) 24.
[56] S. Ouchani, Etude par faisceaux d'ions des effets de la désintegration alpha sur la fluoroapatite, Thesis, University Paris XI, Orsay, 1997.
[57] S. Ouchani, J.C. Dran, J. Chaumont, Nucl. Instrum. and Meth. B 132 (1997) 447.
[58] R. Devanathan, K.E. Sickafus, W.J. Weber, M. Nastasi, J. Nucl. Mater. 253 (1998).